In-line ultrasonic characterization of shear dispersion processes of polydisperse fillers in polymer melts

2002 J. Phys.: Condens. Matter 14 4943

(http://iopscience.iop.org/0953-8984/14/19/317)

INSTITUTE OF PHYSICS PUBLISHING JOURNAL OF PHYSICS: CONDENSED MATTER

J. Phys.: Condens. Matter **14** (2002) 4943–4961 PII: S0953-8984(02)29256-5

In-line ultrasonic characterization of shear dispersion processes of polydisperse fillers in polymer melts

Leïla Haïder[1], Jacques Tatibouët[1], Arnaud Lafaurie[2] and Laurent Ferry[2]

[1] Industrial Materials Institute, National Research Council Canada, 75 de Mortagne, Boucherville, Québec, Canada J4B 6Y4
[2] Centre des Matériaux de Grande Diffusion, École des Mines d'Alès, 06 avenue de Clavières, 30319 Alès Cedex, France

Received 28 September 2001, in final form 25 February 2002
Published 2 May 2002
Online at stacks.iop.org/JPhysCM/14/4943

Abstract

Shear break-up processes of polydisperse fractal clusters are investigated by the ultrasound scattering technique. Within the framework of fractal aggregation and the hybrid approach model for polydisperse correlated scatterers, the concept of variance in the local filler concentration is used to derive a new expression for the scattering cross-section for polydisperse fractal aggregates in the Rayleigh scattering regime. Considering the scaling laws for the shear-induced disruption of the clusters, the shear stress dependence of the ultrasound scattered intensity for polydisperse fractal aggregates is also derived. The fractal scattering regime is further discussed for both monodisperse and polydisperse clusters of size larger than the wavelength. In-line ultrasonic measurements for the shear disruption processes of silica fume fillers compounded with polypropylene during extrusion are investigated. A critical disaggregation shear stress is determined and is found to decrease with the filler surface treatment concentration. This stress is representative of the particle adhesiveness and aggregate dispersion in the matrix. This is confirmed by the improvement in impact resistance tests. On the basis of the scaling laws and the self-consistent-field approximation usually used in the microrheological models, the shear-thinning behaviour of silica fume clusters is successfully simulated.

Nomenclature

f	Ultrasound frequency
λ	Wavelength
$\bar{r}, a$	Particle radii
R	Cluster radius
$\hat{R}$	Maximum size of filling space subclusters at rest
κ_p	Compressibility of the scatterers
κ_0	Compressibility of the suspending medium
ρ_0	Density of the suspending medium
ρ_p	Density of the scatterers
$\vec{k}, \vec{s}$	Incident and scattered wavenumber vectors
n, n_i	Particle numbers per unit of volume
n_a	Cluster number per unit of volume
V, V_i	Particle volumes
V_a	Cluster volume
$\sigma_m, \sigma_p, \sigma_{am}, \sigma_{ap}$	Differential scattering cross-sectional areas
W_m, W_p	Packing factors
m	Critical exponent for cluster break-up
ϕ	Filler volume fraction
ϕ_a	Cluster volume fraction
ϕ_g	Gelation or percolation threshold
$\dot{\gamma}$	Shear rate at the wall
$\dot{\gamma}_c$	Critical disaggregation shear rate
μ, μ_a	Shear viscosities of the suspension
μ_0	Shear viscosity of the matrix polymer
μ_{0m}	Zero-shear-rate viscosity of the polymeric matrix
τ	Shear stress
τ_c	Critical disaggregation shear stress
τ^*	Critical shear stress for cluster break-up
τ_0	Yield stress
α_t	Total attenuation ($\alpha_t = \alpha_{ap} + \alpha_{\mathrm{pol}}$)
α_{pol}	Ultrasonic attenuation in the polymeric matrix
$\alpha_p, \alpha_m, \alpha_{ap}$	Scattering cross-sections per unit of volume
α_r	Dimensionless scattering coefficient ($\alpha_r = \alpha_{ap}/\alpha_p$)
v	Ultrasonic velocity
e	Thickness of the polymeric matrix
w	Angular frequency
$\mathrm{var}(r)$	Normalized variance in size of the particles
$\mathrm{var}_a(R)$	Normalized variance in size of the clusters
$\mathrm{var}(\omega)$	Variance of the particle number in a voxel
ω	Particle number in a voxel
D	Fractal dimension of a cluster
N	Particle number in a cluster
N_b	Number of subunits of size $1/q$ in a cluster
ΔV	Volume of an elemental voxel
q	Scattering wavenumber ($q = s - k$)
S_m, S_p	Structure factors
Γ	Surface adhesive energy
F	Force required to break two particles

1. Introduction

There is a growing of interest in the use of ultrasound as a basis for non-destructive evaluation of media that consist of a homogeneous isotropic continuous phase in which small particles are randomly dispersed. The continuous phase may be liquid, with liquid or solid particles as in food products, paints or lubricants, or both phases may be solid as is the case for filled polymers, particularly adhesives. The use of fillers in thermoplastics to obtain specific properties at low cost is an alternative of considerable interest. Fillers are added to polymer to enhance the mechanical properties such as impact strength, high-temperature creep resistance, stiffness and opacity [1, 2]. Ultrasonic wave propagation in such media is affected by relaxations in the continuous polymer phase as well as by scattering at filler particles [3, 4]. Particle agglomeration influences the scattered power from a dense aggregate of size much smaller than the wavelength (Rayleigh scattering regime) which scales as the square of the cluster volume [5]. Over the last two decades, numerous theoretical models of ultrasound scattering have initiated an upsurge of interest in the prediction of acoustic properties of aggregated suspensions [6–9]. Many of the contributions have been directed at understanding the relationship between the ultrasonic scattered power and filler volume fraction. Little attention has been paid to the ultrasound scattering from a dense distribution of particles or clusters which can no longer be considered as independent scatterers since the increase in correlation among scatterers (particles or aggregates) induces destructive interferences and a decay in the scattered power as the filler volume fraction increases [6]. Moreover, particle size distribution increases the scattered power as the particle volume fraction increases, because of additional scattering arising from polydispersity [10, 11]. Shear disruption processes and multiple hydrodynamic interactions in dense-packed systems further influence both the equilibrium aggregate size and the ultrasonic scattered power [12].

In the present study, shear break-up processes of polydisperse fillers in polymer melts are studied by the ultrasound scattering technique. The first section concerns ultrasound scattering from a dense suspension of polydisperse fillers. Many numerical simulations and experimental works suggest that aggregates behave as fractal on a scale larger than the primary particle size [13]. Taking into account the fractal properties of the clusters and within the framework of the hybrid approach model for mixtures of correlated Rayleigh scatterers [6, 14], we consider the concept of variance in local filler concentration and then we derive a new expression for the scattering cross-section per unit of volume for polydisperse fractal clusters in the Rayleigh scattering regime. On the basis of the mean-field approach proposed by Snabre and Mills [15, 16] giving the scaling laws for the shear break-up of the clusters, we describe the shear stress dependence of the ultrasound scattered intensity for polydisperse fractal aggregates in dense media. The fractal scattering regime is further discussed for clusters of size larger than the wavelength. In a second part, we present experimental results for the shear disruption processes of silica fume aggregates. Chemically treated and untreated silica fumes have been incorporated in polypropylene. In-line ultrasonic measurements were performed during extrusion of the compounds to investigate the effects of filler volume fraction and shear rate. Ultrasonic experiments are discussed on the basis of the scaling laws used. The ability of the ultrasonic scattering method to estimate the critical disaggregation shear stress and to give quantitative information about the particle adhesiveness in relation to the filler surface treatment is discussed. In the last section, ultrasonic results are correlated with impact resistance tests. Using the microrheological model based on the mean-field approximation [15, 16] and the estimates of the critical shear stress, we then describe the shear-thinning behaviour of untreated silica fume aggregates during extrusion.

2. Ultrasound scattering theory

2.1. Uncorrelated monodisperse scatterers

Ultrasound scattering from particles arises from the different modes of vibrations in relation either to compressibility or density mismatches. A mismatch in compressibility causes the obstacle to pulsate (expand and contract), whereas a mismatch in density causes the obstacle to oscillate back and forth about the undisturbed position [5]. The Green function approach gives the differential scattering cross-section $\sigma_m(\vec{k}, \vec{s})$ of a weak Rayleigh scatterer of average size $\bar{r}$, volume V and arbitrary shape [17]:

$$\sigma_m(\vec{k}, \vec{s}) = pV^2(\bar{r}) \tag{1}$$

with

$$p = \pi^2 f^4 (\kappa_0 \rho_0)^2 \left[\left(\frac{\kappa_p - \kappa_0}{\kappa_0} \right) + \left(\frac{\rho_p - \rho_0}{\rho_p} \right) \frac{\vec{k} \cdot \vec{s}}{ks} \right]^2 \tag{2}$$

where f is the ultrasound frequency, κ_p, κ_0 and ρ_p, ρ_0 are the compressibilities and densities of the scatterer and suspending medium, respectively and $\vec{k}$, $\vec{s}$ are the scattered wavenumber vectors. The ultrasonic scattering coefficient $\alpha_m(\vec{k}, \vec{s})$ defined as the power scattered per unit solid angle from a unit volume for an incident plane wave of unit amplitude then scales as the average number n of the scatterers per unit volume [18]:

$$\alpha_m(\vec{k}, \vec{s}) \approx n\sigma_m(\vec{k}, \vec{s}). \tag{3}$$

2.2. Uncorrelated polydisperse scatterers

For mixtures of n_i similarly shaped but differently sized particles (r_i for $i = 1$–N), of volume V_i, we consider the net filler volume fraction $\phi = \sum n_i V_i = n \sum (n_i/n) V_i \equiv n\langle V \rangle$ of the polydisperse scatterers to give an equation analogous to (3), which is therefore given by

$$\alpha_p(\vec{k}, \vec{s}) \approx p \sum n_i V_i^2 = np \sum \left(\frac{n_i V_i^2}{n} \right) = n\sigma_p(\vec{k}, \vec{s}), \tag{4}$$

where the corresponding low-frequency scattering cross-sectional area $\sigma_p(\vec{k}, \vec{s})$ scales as [10, 11]

$$\sigma_p(\vec{k}, \vec{s}) = p \sum \left(\frac{n_i V_i^2}{n} \right) \approx p\langle V^2 \rangle. \tag{5}$$

In the framework of a continuous size distribution governed by Poisson probability functions whose skewness depends on the normalized variance in size $\mathrm{var}(r) = (\langle r^2 \rangle - \bar{r}^2)\bar{r}^2$ of the scatterers, the ultrasonic scattering cross-sectional area $\sigma_p(\vec{k}, \vec{s})$ thus becomes

$$\sigma_p(\vec{k}, \vec{s}) \approx p \frac{\langle V^2 \rangle}{\langle V \rangle} \langle V \rangle = \sigma_m(\vec{k}, \vec{s})(1 + \mathrm{var}(r))(1 + 2\,\mathrm{var}(r)) \cdots (1 + 5\,\mathrm{var}(r)). \tag{6}$$

The low-frequency scattered power $\alpha_p(\vec{k}, \vec{s})$ from polydisperse uncorrelated scatterers per unit of volume in the Rayleigh scattering regime then scales as [11]

$$\alpha_p(\vec{k}, \vec{s}) \approx n\sigma_m(\vec{k}, \vec{s})(1 + \mathrm{var}(r))(1 + 2\,\mathrm{var}(r)) \cdots (1 + 5\,\mathrm{var}(r)). \tag{7}$$

Particle size distribution influences the scattering behaviour of individual polydisperse scatterers and induces an increase of the scattering cross-section per unit of volume because of additional scattering arising from polydispersity.

2.3. Mixtures of correlated scatterers

Departure from independent scattering occurs in densely packed systems where the scatterers can no longer be treated as independent since proximity effects and correlation effects lower the ultrasonic scattered power because of destructive interference of the wavelets arising from a dense distribution of scatterers [19, 20].

Within the framework of the particle approach, coherent addition of the scattered waves leads to the ultrasonic scattering coefficient $\alpha_p(\vec{k}, \vec{s})$:

$$\alpha_p(\vec{k}, \vec{s}) = n\sigma_p(\vec{k}, \vec{s})W_p(\vec{k}, \vec{s}) = np\langle V^2\rangle W_p(\vec{k}, \vec{s}) \tag{8}$$

where $W_p(\vec{k}, \vec{s})$ is the packing factor derived from the Percus–Yevick pair correlation for mixtures, accounting for dependent scattering in dense systems [10, 11]. The packing factor is contingent on the selection of an appropriate pair correlation function depending on particle volume fraction, particle shape, particle size distribution and flow conditions. Assuming polydisperse scatterers and no shear dependence of the pair correlation function, the packing factor $W_p(\phi)$ is given by

$$W_p(\phi) = W_m(\phi)\left[1 + \frac{\phi}{(1-\phi)}\frac{12\,\mathrm{var}(r)}{(1+5\,\mathrm{var}(r))} + \frac{\phi^2}{(1-\phi)^2}\frac{9\,\mathrm{var}(r)}{(1+4\,\mathrm{var}(r))}\right] \tag{9}$$

where $W_m(\phi) = (1-\phi)^4/(1+2\phi)^2$ represents the packing factor for the monodisperse case [14]. The primary effects of polydispersity as shown in figure 1 are to increase the scattered power per unit of volume and to reduce the fall-off as the filler volume fraction increases. The packing factor viewpoint further involves complex statistical mechanics and provides some physical insight [10, 11]. One may thus consider an alternative viewpoint derived from the hybrid approach [6, 14] and based on the concept of variance in local particle volume fraction. This approach sums the wavelets from elemental volumes of size $\approx\lambda/2\pi$ (the voxel), small enough that the incident wave arrives with the same phase at every particle located within it. The scattered power can be split into a part arising from a 'crystalline' phase which gives no net contribution because of destructive wave interference and another representing contributions from independent fluctuations in the particle number ω within the elemental voxel of volume ΔV and size $\approx 1/k$. The low-frequency scattered power from a dense suspension then scales as the variance $\mathrm{var}(\omega) = \omega^2 - \overline{\omega}^2$ of the particle number ω within a voxel [6, 14]:

$$\alpha_p(\vec{k}, \vec{s}) = n\sigma_p(\vec{k}, \vec{s})(\mathrm{var}(\omega)/\omega) = np\langle V^2\rangle(\mathrm{var}(\omega)/\omega) \tag{10}$$

with $n = \omega/\Delta V$

2.4. Irreversible fractal clusters

Several models of random cluster growth developed in the last decade suggest that aggregates behave as fractal on a scale larger than the primary particle size. Computer simulation led to self-similar clusters with radius of gyration obeying the scaling relationship [13]

$$R(N) \approx \bar{r}N^{1/D} \tag{11}$$

where N is the number of particles in the fractal cluster, $\bar{r}$ the characteristic radius of elementary particles and D the fractal dimension. A fractal dimension less than the Euclidean dimension d corresponds to open floc structures with porosity increasing with size.

Within the framework of a fractal homogeneous aggregation, recent works by Snabre and co-workers [12, 23, 24] show that ultrasonic scattering from a Rayleigh cluster ($Rk \ll 1$) is

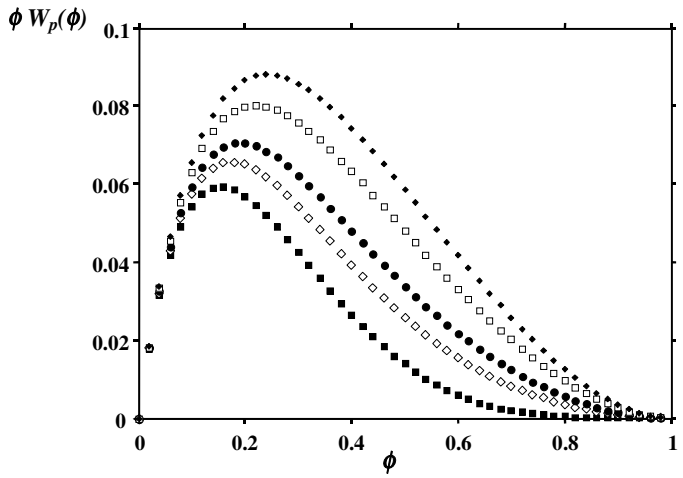

Figure 1. A plot of the packing factor times the particle volume fraction $\phi W_p(\phi)$ versus the filler volume fraction with $\mathrm{var}(r) = 0$ (■), $\mathrm{var}(r) = 0.05$ (◇), $\mathrm{var}(r) = 0.1$ (●), $\mathrm{var}(r) = 0.25$ (◇) and $\mathrm{var}(r) = 0.5$ (♦).

coherent and that the scattering cross-sectional area $\sigma_{am}(\vec{k}, \vec{s})$ of a cluster of arbitrary shape is proportional to the square of the particle number N within the aggregates:

$$\sigma_{am}(\vec{k}, \vec{s}) \approx N^2 \sigma_m(\vec{k}, \vec{s}). \tag{12}$$

For continuous distributions of the clusters, taking $\langle R^2 \rangle = \langle r^2 \rangle N^{2/D}$ one may consider the normalized variance in size $\mathrm{var}_a(R)$ of the aggregates which scales as the normalized variance $\mathrm{var}(r)$ of individual scatterers:

$$\mathrm{var}_a(R) = \frac{\langle R^2 \rangle - \overline{R}^2}{\overline{R}^2} \approx \frac{\overline{r}^2 N^{2/D}[1 + \mathrm{var}(r)] - \overline{r}^2 N^{2/D}}{\overline{r}^2 N^{2/D}} = \mathrm{var}(r) \tag{13}$$

and then we derive the ultrasonic scattering cross-sectional area $\sigma_{ap}(\vec{k}, \vec{s})$ of a fractal aggregate of N polydisperse particles within the fractal structure:

$$\sigma_{ap}(\vec{k}, \vec{s}) \approx p\langle V_a^2 \rangle \approx p\left(\frac{\langle V_a^2 \rangle}{\langle V_a \rangle}\right)\langle V_a \rangle \qquad \text{for } k\bar{r}N^{1/D} \ll 1 \tag{14}$$

with

$$\langle V_a^2 \rangle / \langle V_a \rangle = \langle V_a \rangle \frac{(1 + 3\,\mathrm{var}(r))(1 + 4\,\mathrm{var}(r))(1 + 5\,\mathrm{var}(r))}{(1 + \mathrm{var}(r))(1 + 2\,\mathrm{var}(r))} \tag{15}$$

and

$$\langle V_a \rangle = V_a(\overline{R})(1 + \mathrm{var}(r))(1 + 2\,\mathrm{var}(r)). \tag{16}$$

Substituting for the ratio $(\langle V_a^2 \rangle / \langle V_a \rangle)$ and the average volume $\langle V_a \rangle$ of a cluster in equation (14), the ultrasonic scattering cross-sectional area $\sigma_{ap}(\vec{k}, \vec{s})$ for a fractal cluster scales as

$$\sigma_{ap}(\vec{k}, \vec{s}) \approx N^2 \sigma_m(\vec{k}, \vec{s})(1 + \mathrm{var}(r))(1 + 2\,\mathrm{var}(r)) \cdots (1 + 5\,\mathrm{var}(r)). \tag{17}$$

According to the hybrid approach model for mixtures of correlated Rayleigh aggregates [12, 23], the ultrasonic scattering coefficient $\alpha_{ap}(\vec{k}, \vec{s})$ is therefore given by

$$\alpha_{ap}(\vec{k}, \vec{s}) \approx n_a \sigma_{ap}(\vec{k}, \vec{s})\left(\frac{\mathrm{var}_a(\omega)}{\omega}\right) \tag{18}$$

where $\mathrm{var}_a(\omega)$ is the variance of the particle number ω in a voxel, $n_a = n/N$ the number of clusters per unit volume. Cluster growth increases the variance in particle number because each voxel can gain or lose a large number of elementary particles. At a first approximation, the variance $\mathrm{var}_a(\omega)$ increases linearly with the volume fraction ϕ_a of the aggregates and can be reasonably approximated by [12, 23]

$$\mathrm{var}_a(\omega) \approx \frac{\phi_a}{\phi}\,\mathrm{var}(\omega) \qquad \text{for } N \ll (k\bar{r})^{-D}. \tag{19}$$

Then,

$$\alpha_{ap}(\vec{k},\vec{s}) \approx n_a N^2 \left(\frac{\phi_a}{\phi}\right)\sigma_m(\vec{k},\vec{s})\left(\frac{\mathrm{var}(\omega)}{\omega}\right)(1+\mathrm{var}(r))(1+2\,\mathrm{var}(r))\cdots(1+5\,\mathrm{var}(r)). \tag{20}$$

We further define the ultrasonic normalized scattering coefficient $\alpha_r = \alpha_{ap}(\vec{k},\vec{s})/\alpha_p(\vec{k},\vec{s})$. Using equations (10) and (20), the dimensionless ultrasonic scattering coefficient α_r then becomes

$$\alpha_r(\vec{k},\vec{s}) = \frac{\alpha_{ap}(\vec{k},\vec{s})}{\alpha_p(\vec{k},\vec{s})} = \left(\frac{n_a}{n}\right)\left(\frac{\phi_a}{\phi}\right)N^2 = \left(\frac{R}{a}\right)^3 \qquad \text{for } k\bar{r}N^{1/D} \ll 1 \tag{21}$$

where

$$\frac{\phi_a}{\phi} = \frac{n_a\langle V_a\rangle}{n\langle V\rangle} = \left(\frac{1}{N}\right)\left(\frac{V_a(\overline{R})}{V(\overline{r})}\right)\left[\frac{(1+\mathrm{var}_a(R))(1+2\,\mathrm{var}(R))}{(1+\mathrm{var}(r))(1+2\,\mathrm{var}(r))}\right] = \left(\frac{1}{N}\right)\left(\frac{V_a(\overline{R})}{V(\overline{r})}\right). \tag{22}$$

The ultrasonic normalized scattering power is nearly isotropic in the Rayleigh scattering regime and scales as the average volume $V_a(\overline{R})$ of clusters with no significant dependence on the filler volume fraction and particle size distribution.

Far-field coherence effects and particle size distribution together determine the cluster volume dependence of the scattering coefficient α_r. One can indeed expect no influence of the fractal dimension of clusters upon the scattering coefficient α_r because the transducer cannot resolve the internal structure of aggregates smaller than voxels. As a consequence, the dimensionless scattering coefficient α_r can be interpreted as an aggregation index in the Rayleigh scattering regime.

2.5. The fractal scattering regime

For aggregates of dimension larger than a voxel ($kR \gg 1$), the hybrid approach is no longer valid and ultrasound scattering becomes strongly anisotropic because of angle-dependent destructive interferences. Considering the scattering wavenumber $q = s - k$, the choice of a scattering angle θ sets a length scale $1/q = [2k\sin(\theta/2)]^{-1}$ under which scattering remains coherent. Therefore one may decompose an aggregate into smaller subunits or blobs of size $\approx 1/q$ with a number $N_b \approx (qa)^{-D}$ of elementary particles. One subunit scatters coherently a power scaling as N_b^2. In contrast, the scattered waves from different subunits add incoherently and the differential scattering cross-section $\sigma_a(\vec{k},\vec{s})$ of arbitrary-shape aggregates scales as the number N/N_b of subunits in the cluster [12, 23]:

$$\sigma_{am}(\vec{k},\vec{s}) \approx \left(\frac{N}{N_b}\right)N_b^2\sigma_m(\vec{k},\vec{s}) \approx N^2 S_m(qR)\sigma_m(\vec{k},\vec{s}) \tag{23}$$

where $S_m(qR) \approx N_b/N \approx (qR)^{-D}$ is commonly referred to as the structure factor in coherent optics and describes spatial correlations between particles in fractal structures [25, 26]. The fourth-order frequency law characterizing the Rayleigh scattering regime no longer applies for clusters larger than a voxel ($\sigma_{am}(\vec{k},\vec{s}) \approx a^6 R^{-D}\lambda^{D-4}$).

In the case of polydisperse distributions, the differential scattering cross-sectional area involves an effective structure factor $S_p(qR)$ accounting for polydispersity effects and scaling as

$$S_p(qR) \approx (qR)^{-D}(1+\mathrm{var}(r))(1+2\,\mathrm{var}(r))\cdots(1+5\,\mathrm{var}(r))$$
$$\approx S_m(qR)(1+\mathrm{var}(r))(1+2\,\mathrm{var}(r))\cdots(1+5\,\mathrm{var}(r)). \quad (24)$$

The low-frequency scattering cross-sectional area $\sigma_{ap}(\vec{k},\vec{s})$ thus becomes

$$\sigma_{ap}(\vec{k},\vec{s}) \approx N^2 S_p(qR)\sigma_m(\vec{k},\vec{s})$$
$$\approx N^2 S_m(qR)(1+\mathrm{var}(r))(1+2\,\mathrm{var}(r))\cdots(1+5\,\mathrm{var}(r))\sigma_m(k,s). \quad (25)$$

For large clusters ($qR \gg 1$), the directional scattering cross-section $n_a\sigma_{ap}(\vec{k},\vec{s})$ per unit of volume then scales as

$$\alpha_{ap}(\vec{k},\vec{s}) \approx \frac{\phi}{\langle V\rangle}(qa)^{-D}\sigma_m(\vec{k},\vec{s})(1+\mathrm{var}(r))(1+2\,\mathrm{var}(r))\cdots(1+5\,\mathrm{var}(r)) \quad (26)$$

$$\approx \frac{\phi}{V(\bar{r})}(qa)^{-D}\sigma_m(\vec{k},\vec{s})(1+3\,\mathrm{var}(r))(1+4\,\mathrm{var}(r))(1+5\,\mathrm{var}(r)). \quad (27)$$

In the fractal scattering regime ($kR \gg 1$), the dimensionless ultrasonic scattering coefficient $\alpha_r = \alpha_{ap}/\alpha_{p} \approx (qa)^D(1+3\,\mathrm{var}(r))(1+4\,\mathrm{var}(r))(1+5\,\mathrm{var}(r))/W(\phi)$ mainly involves the scattering angle and fractal dimension of the clusters and thus becomes sensitive to the internal structure of the aggregates and therefore to the polydispersity of the scatterers. The normalized scattered power per unit of volume is no longer sensitive to the cluster size and as a consequence can no longer characterize the aggregation state of a suspension.

3. Shear break-up of fractal clusters

3.1. Equilibrium size of the aggregates in shear flow

Above a critical yield stress, the shear-thinning behaviour of aggregated suspensions results from the rupture of the spanning network and finite clusters when increasing the shear stress. Clusters can grow in a shear field until they reach a maximum stable size corresponding to a dynamical equilibrium between formation and shear break-up of the aggregates [15, 27–34]. An aggregate with radius above the maximum stable size is disrupted by shear stresses. As shown by experimental investigations [29] and computer simulations [35, 36], the shear stress dependence of the equilibrium radius $R(\tau)$ of an isolated fractal cluster obeys the general power law

$$\frac{R(\tau)}{\bar{r}} \approx \left(\frac{\tau^*}{\tau}\right)^m \qquad \text{with } 0.3 < m < 0.5 \quad (28)$$

where the critical shear stress $\tau^* \approx \Gamma/a$ for cluster break-up is related to the surface adhesive energy Γ (adhesive energy per unit contact area) and the characteristic radius $\bar{r} = a$ of elementary particles. The fragility of bonds depends on the reversibility of cluster deformation under the action of external stresses [35, 37]. Soft and rigid clusters represent extreme possible behaviour of the aggregates. Rigid clusters are more probably broken into secondary aggregates of approximately equal parts (the *large-scale fragmentation process*) since elastic deformations are transmitted over the whole structure. On the other hand, soft structures are irreversibly deformed by external stresses and splits of individual particles and small clusters one by one until the cluster reaches a stable size (the *surface erosion process*) [15, 35].

We may thus consider the mean-field approach proposed by Snabre and Mills [15] giving a scaling law similar to the phenomenological equation (28) with $m = 1/2$ for deformable aggregates and $m = 1/3$ for rigid clusters.

We introduce a correlation length ξ under which elastic stresses are transmitted and consider the cluster as a soft assembly of rigid subunits of radius ξ [15]. A three-dimensional cluster of fractal dimension $D \geqslant 2$ strongly interacts with the surrounding fluid and roughly behaves hydrodynamically like an impermeable compact sphere with a hydrodynamic radius close to the radius of gyration [37]. An impermeable cluster of size R further experiences a viscous force:

$$F = \int \bar{\bar{\tau}}\, \mathrm{d}s = \tau R^2 \tag{29}$$

where $\bar{\bar{\tau}}$ is the viscous stress tensor and $\mathrm{d}s$ an outer surface element. This shear force exerts a bending moment $M = F\xi$ on the rigid branches of size ξ located on the outer surface of the cluster. A bending moment higher than the critical moment $M^* \approx \tau^* a^3 \approx \Gamma a^2$ for breaking a cluster leads to the rupture of rigid subunits. The breaking criterion $F\xi = \Gamma a^2$ and the characteristic shear stress for cluster break-up then give the maximal stable size $R(\tau)$:

$$R(\tau) \approx \left(\frac{\Gamma a^2}{\tau \xi}\right)^{1/2}. \tag{30}$$

For soft clusters, outer chains of size $\xi \approx a$ are stretched one by one until the cluster reaches the maximal stable size $R(\tau)$:

$$\frac{R(\tau)}{a} \approx \left(\frac{\tau^*}{\tau}\right)^{1/2} \qquad \text{with } \tau^* \approx \Gamma/a. \tag{31}$$

In the case of rigid structures, the correlation length is the same order as the whole size of the radius of the aggregate and then this structure is broken into equal parts:

$$\frac{R(\tau)}{a} \approx \left(\frac{\tau^*}{\tau}\right)^{1/3} \qquad \text{with } \tau^* \approx \Gamma/a. \tag{32}$$

Equations (31) and (32) for soft and rigid aggregates give the upper and lower bound of the exponent m in the general law (28). On one hand, for a weak bonding energy (reversible aggregation), recent computer simulations of the shear-induced disruption of three-dimensional soft aggregates give $m = 1/2$ [29]. On the other hand, the lower value $m = 1/3$ agrees well with experimental data from Torres *et al* [36] for rigid clusters in relation to irreversible flocculation (strong bonding energy).

3.2. Ultrasonic scattering from irreversible fractal clusters in shear flow

We can now derive the shear stress dependence of the ultrasound scattering cross-section per unit of volume from a dense suspension of Rayleigh polydisperse fractal clusters. Considering both the cluster volume dependence of the scattered power per unit of volume (equation (21)) and the scaling law for the shear break-up of the clusters (equation (28)), the dimensionless ultrasonic scattering coefficient $\alpha_r(\tau)$ then obeys the power law

$$\alpha_r(\tau) = \left(\frac{R(\tau)}{a}\right)^3 \approx 1 + \left(\frac{\tau^*}{\tau}\right)^{3m} \qquad \text{for } kR \ll 1 \tag{33}$$

where particle adhesiveness and cluster deformability respectively determine the critical shear stress τ^* for cluster break-up and the exponent m. In the Rayleigh scattering regime, the particle volume fraction within the aggregates, the particle size distribution and the fractal dimensionality have no influence on the size of Rayleigh clusters and therefore on the dimensionless ultrasonic scattering coefficient.

4. Ultrasonic scattering from silica fume aggregates

4.1. Silica-fume-filled polypropylene

Silica fumes are a by-product of the silicon or ferrosilicon industry when production is in electric furnaces. Raw silica fume waste from a silicon plant (Péchiney Electrométallurgie, France) was used as fillers to increase the stiffness of thermoplastic polymers, especially polypropylene. Silica fumes have a particle average size of 50 nm and a specific surface area of 20 $m^2\ g^{-1}$. Polypropylene used in compounding (PP3400MA1 from APPRYL) has a melt flow index of 40 g/10 min.

4.2. Experimental procedure

Rheo-acoustic experiments were performed for silica fume aggregates dispersed in a PP homopolymer at 30 wt% loading. Ultrasonic measurements were first performed in static mode [38, 39] (figure 2(*a*)). The polymer with known thickness e was confined between two aligned steel rods at the opposite end of which the ultrasonic transducers were attached. Ultrasonic properties of the confined polymer were obtained under controlled pressure (P) and temperature (T). Longitudinal waves were then produced with piezoelectric transducers at a frequency of 2.68 MHz. The generating transducer sends a burst of sound propagating down the transmission line. At the steel/polymer interface, one part of the energy was transmitted into the polymer; there the pulse travelled with a characteristic velocity v, while its amplitude decreased with path length, z, according to $\exp(-\alpha_t z)$, where α_t is the total attenuation resulting from relaxation mechanisms in the polymeric matrix and scattering by fillers. On reaching the second interface, part of the energy crossed over and was detected by the receiving transducer. The remainder of the energy reverberated in the polymer until completely damped, giving rise to a series of echoes, A_1, A_2, A_3. The ultrasonic attenuation α_t, which measures both the mechanical energy lost to the polymer α_{pol} and the scattering fraction α_{ap} from the fillers of size much smaller than the wavelength, was calculated from the amplitude ratio of successive echoes, and defined on a logarithmic scale in dB as $\alpha_t = \alpha_{ap} + \alpha_{\mathrm{pol}} = 10[\log(A_1/A_2)]/e$ while the ultrasonic velocity was determined from the time delay Δt, for a round trip, between successive echoes $v = 2e/\Delta t$.

The ultrasonic technique was adapted for in-line monitoring [39]. For this purpose, ultrasonic probes are fitted to an extrusion slit die (figure 2(*b*)) to generate pulses of ultrasound across the thickness e of the flowing melt (resonance frequency of the transducers $f = 5$ MHz). In that case, the whole polymer flow is characterized at a rate as high as five times per second. The die is also equipped with thermocouples for measuring both die temperature T_{Die} and melt temperature T_{Melt}, and pressure sensors for describing the pressure profile along the flow and hence the pressure P near the ultrasonic probes and the shear stress at the wall. The signals are digitized and the ultrasonic parameters are extracted using specialized high-speed signal analysis algorithms.

4.3. Shear break-up of silica fume aggregates

Silica fume particles exhibit a strong tendency to form aggregates. Particle flocculation results in an increase of the scattering coefficient $\alpha_{ap} = \alpha_t - \alpha_{\mathrm{pol}}$ which scales as the square of the cluster volume. Ultrasonic measurements in static mode were done on four compounds with different filler concentration. Ultrasonic attenuation due to the scattering is shown in figure 3 as a function of the silica fume volume fraction. The attenuation increases up to around $\phi \approx 20\%$ as the particle volume fraction increases. Departure from uncorrelated scatterers

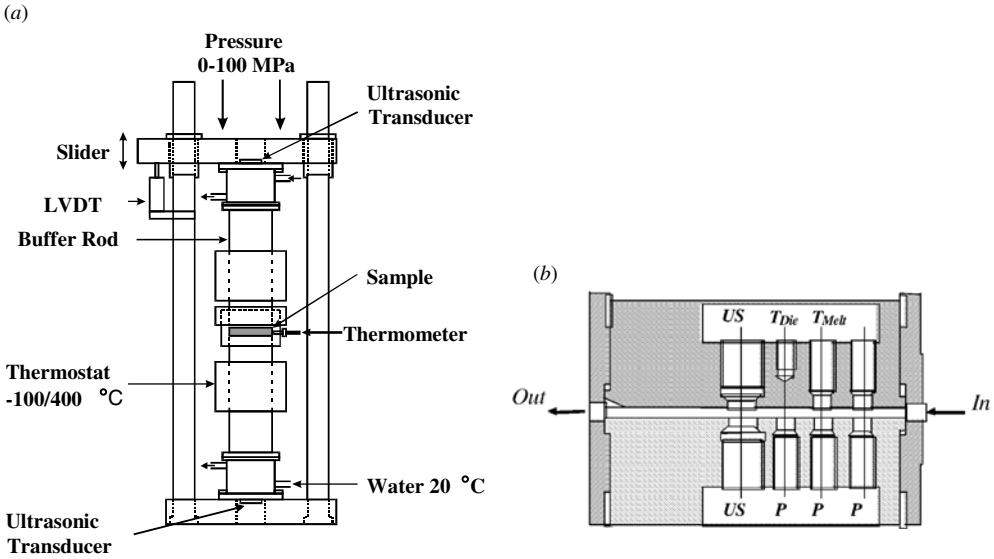

Figure 2. (*a*) The experimental ultrasonic device used for static mode experiments. (*b*) The experimental ultrasonic instrumented die with ultrasonic transducer (US), pressure probes (P) and both die and melt thermocouples (T_{Die} and T_{Melt}).

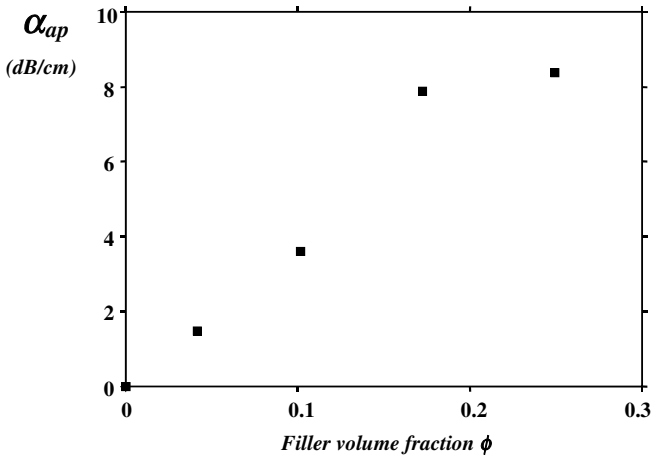

Figure 3. Ultrasonic attenuation α_{ap} in static mode due to scattering from untreated silica fume aggregates in suspension in polypropylene versus filler volume fraction ϕ ($T = 160\,^{\circ}\mathrm{C}$ and $P = 100$ bar).

occurs for higher filler concentration as indicated by the last experimental value. This result is in agreement with the evolution of the packing factor described in figure 1. Larger filler concentrations are needed to observe the attenuation decrease attributed to correlated scatterers.

Ultrasonic experiments were performed during the extrusion of two compounds to investigate the shear break-up processes of silica fume aggregates. The screw speed was increased step by step and both the attenuation and velocity were monitored when the steady state was reached, with pressure profiles in the die. Mass throughput measurements were

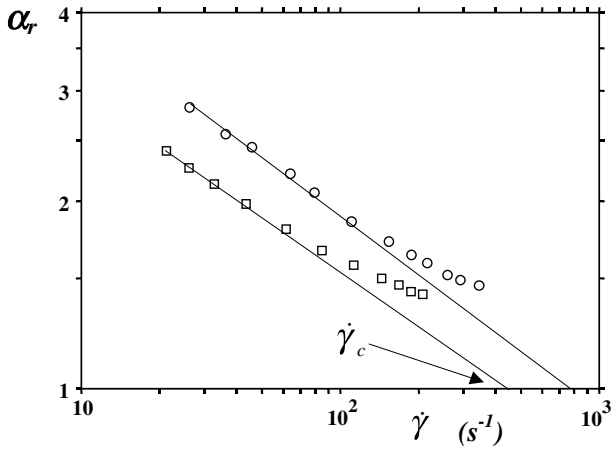

Figure 4. Dimensionless ultrasonic scattering coefficient α_r versus the wall shear rate $\dot{\gamma}$ for untreated silica fume particles in polypropylene. Filler volume fraction $\phi = 0.08$ (○) and $\phi = 0.17$ (□). $T = 205\,^{\circ}$C.

Table 1. Experimental values of the critical disaggregation shear rate $\dot{\gamma}_c$, shear viscosity $\mu(\dot{\gamma}_c)$ and critical shear stress τ_c for two silica fume compounds (not treated particles) with polypropylene (volume concentration ϕ).

ϕ	$\dot{\gamma}_c$ (s^{-1})	$\mu(\dot{\gamma}_c)$ (Pa s)	τ_c (kPa)
0.08	712	98.2	69.91
0.17	445	156.6	69.68

done to determine the shear rate at the wall for each rpm step, using the classical relationship $\dot{\gamma} = 6Q/lh^2$, where Q, l, h are respectively the volume throughput, the width and the thickness of the die. A Rabinovitch-type correction was applied to take into account the non-Newtonian behaviour of the polymer melt, using the wall shear stress determination from the pressure profile [40]. The die gap thickness was 1 mm and the die temperature was set to 205 °C.

The dimensionless ultrasonic scattering coefficient $\alpha_r = \alpha_{ap}/\alpha_p$ was determined after the dynamical equilibrium state was reached and plotted as a function of the wall shear rate $\dot{\gamma}$ (figure 4). The normalized scattering coefficient α_r decreases when increasing the shear rate $\dot{\gamma}$ because of the shear break-up of silica fume aggregates into smaller ones. The critical disaggregation shear rate $\dot{\gamma}_c$ was then defined in terms of the extrapolated intercept [12, 15, 23]. The local shear field around the particles and the critical disaggregation shear rate $\dot{\gamma}_c$ are strongly influenced by multiple hydrodynamic interactions in a dense suspension. Under defined shear rate conditions, particle crowding does indeed increase the viscosity of the suspension, resulting in a more efficient dispersion of aggregates and a lower scattering coefficient. Raising the particle volume fraction ϕ then shifts the critical shear rate $\dot{\gamma}_c(\phi)$ towards lower values [12, 15, 23]. Table 1 summarizes the critical parameters for the two compounds.

The critical shear stress τ_c defined as the product of the critical shear rate $\dot{\gamma}_c$ and the shear viscosity $\mu(\dot{\gamma}_c)$ no longer depends on the filler volume fraction (table 1). The critical disaggregation shear stress $\tau_c \approx 69 \times 10^4$ N m^{-2} is indeed representative of the mechanical force required to disrupt bonds between silica fume particles [12, 15, 23]. From the Derjaguin

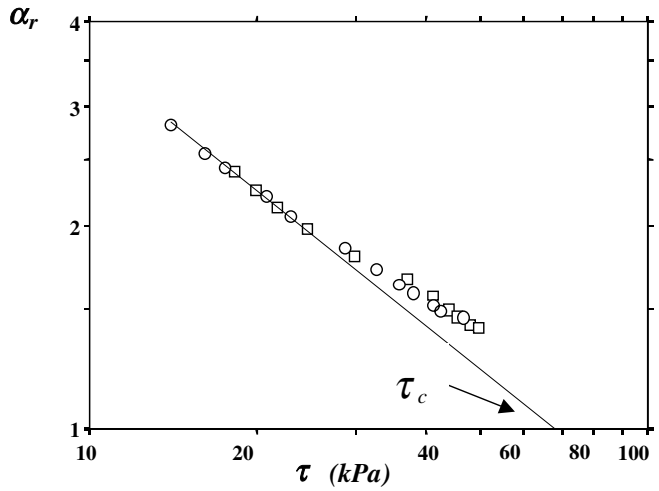

Figure 5. Dimensionless ultrasonic scattering coefficient $\alpha_r = \alpha_{ap}/\alpha_p$ versus the shear stress $\tau = \mu_a(\dot\gamma)\dot\gamma$ for untreated silica fume particles in polypropylene. Filler volume fraction $\phi = 0.08$ (○) and $\phi = 0.17$ (□). $T = 205\,^\circ$C.

theory [40], the force $F \approx \tau_c a^2$ which is required to break a bond between two aggregated particles scales as Γa (Γ is the surface adhesive energy). For untreated silica fume particles ($\tau_c \approx 69 \times 10^4$ N m^{-2} and $\bar r = a \approx 50$ nm), the surface adhesive energy is estimated to be $\Gamma \approx \tau^* a \approx 3.45 \times 10^{-2}$ N m^{-1}.

The effective-medium approximation used in the microrheological models [15] states that interacting aggregates behave like isolated clusters in a fluid of viscosity equal to the shear viscosity of the suspension and thus experience an effective shear stress $\tau = \mu_a(\dot\gamma)\dot\gamma$. Therefore we have plotted in figure 5 the dimensionless scattering coefficient $\alpha_r(\tau)$ against the shear stress $\tau = \mu_a(\dot\gamma)\dot\gamma$ to account correctly for the microrheological conditions around the clusters whatever the particle concentration. Experimental data for the normalized scattering coefficient $\alpha_r(\tau)$ then lie on a single curve since the local shear stress determines the equilibrium size of interacting aggregates. The master curve $\alpha_r(\tau)$ further indicates that correlation effects among individual particles or small aggregates only involve the average particle volume fraction, since the transducer cannot resolve aggregates smaller than a voxel [12, 23].

Silica fume aggregates can be considered as rigid clusters of fractal dimension $D \approx 2$ since small elastic deformations are transmitted over the whole structure and then preserve the structure of rigidly connected particles in relation to irreversible aggregation [15, 33]. We may thus estimate the dimensionless scattering coefficient $\alpha_r(\tau)$ from equation (33) with $m = 1/3$. Taking a characteristic shear stress $\tau^* = \tau_c/3$, relation (33) describes well the shear stress dependence of the dimensionless scattering coefficient $\alpha_r(\tau)$ as shown in figure 6.

In the case of moderate ultrasound frequency such that the wavelength is much larger than the clusters, rheo-ultrasonic experiments provide a way to estimate the characteristic size of the aggregates and to gain quantitative information about the critical disaggregation shear stress which is representative of the particle adhesiveness [12, 23, 24]. For this purpose four compounds corresponding to silica fumes treated with different concentrations of hydrogenated tallow amine were investigated. As shown in figures 7 and 8 as the coating of hydrogenated tallow amine is added, both the ultrasonic scattering power and the critical disaggregation shear stress decrease, before levelling off at higher amine concentration (figure 9). Chemical

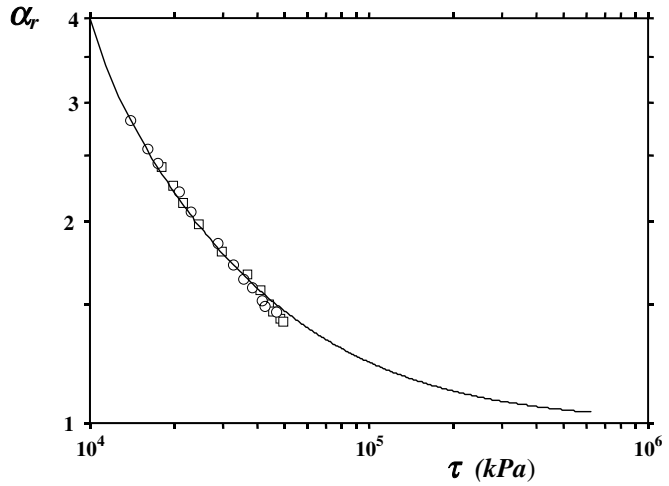

Figure 6. Dimensionless ultrasonic scattering coefficient $\alpha_r = \alpha_{ap}/\alpha_p$ versus the shear stress $\tau = \mu_a(\dot{\gamma})\dot{\gamma}$ for untreated silica fume particles incorporated in PP. Filler volume fraction $\phi = 0.08$ (○) and $\phi = 0.17$ (□). $T = 205\,^{\circ}$C. The solid curve is calculated from the rheo-acoustic model $\alpha_r \approx 1 + (\tau^*/\tau)^{3m}$ with $m = 1/3$ for rigid clusters.

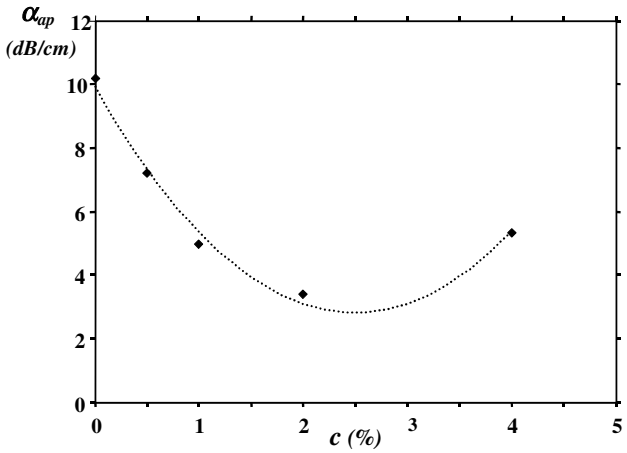

Figure 7. Ultrasonic attenuation α_{ap} due to scattering from silica fume aggregates treated with fatty amine in suspension in polypropylene versus the coating level of hydrogenated tallow amine c (%). $T = 205\,^{\circ}$C and $P = 100$ bar. Filler volume fraction $\phi = 0.17$.

treatments with amine allow a better dispersion of silica fume aggregates. Hydrogenated tallow amine treatment of the filler further enhances the electrostatic repulsive interaction forces and thus reduces the cohesive forces between particles. Conversely, on plotting the impact resistance versus the coating level of hydrogenated tallow amine c (%) (figure 10), we further obtain a curve which increases as the coating is added, indicating a better dispersion of suspension around c (%) $= 3$.

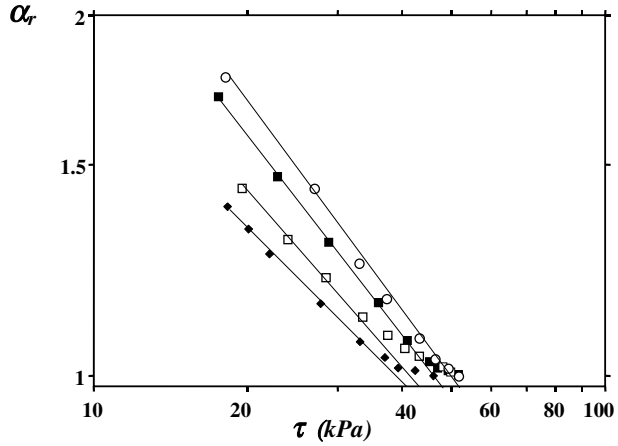

Figure 8. Dimensionless ultrasonic scattering coefficient $\alpha_r = \alpha_{ap}/\alpha_p$ versus the shear stress $\tau = \mu_a(\dot{\gamma})\dot{\gamma}$ for silica fume particles treated with hydrogenated tallow amine in PP. Fatty amine concentration $c = 0.5\%$ (○), $c = 1\%$ (■), $c = 2\%$ (□) and $c = 4\%$ (♦). Filler volume fraction $\phi = 0.17$ and $T = 205\,^{\circ}$C.

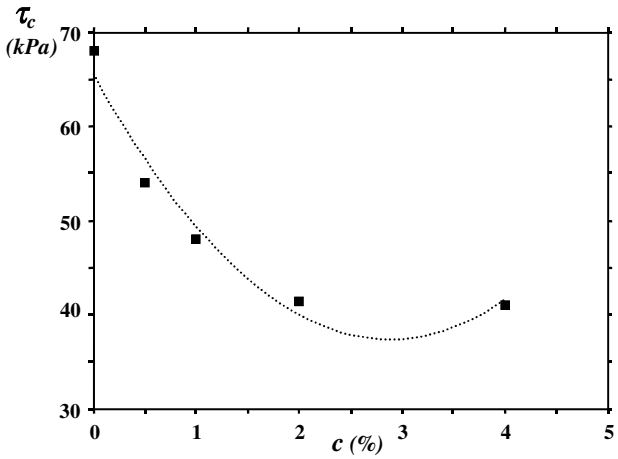

Figure 9. Critical disaggregation shear stresses τ_c determined from the ultrasonic scattering experiments versus the hydrogenated tallow amine concentration c (%).

5. Shear viscosity of aggregated suspensions

The rheology of multi-phase polymeric systems is a very complex subject. During the last four decades statistical models of polymer entanglement [41] and random cluster growth [21, 42] have initiated an upsurge of interest in the rheological properties of aggregated colloids. Within the framework of fractal aggregation, mean-field theories of growth and rupture of fractal clusters were first proposed by Mills and Snabre [27, 28], Sonntag and Russel [29] and Patel and Russel [30]; they indicated a power-law dependence of the viscosity on the shear rate. For aggregated colloidal dispersions, the microrheological models usually assume the effective-medium approximation, in which the viscosity of the medium around a cluster is the viscosity of the suspension, and differ from each other in the rheological laws used for hard-

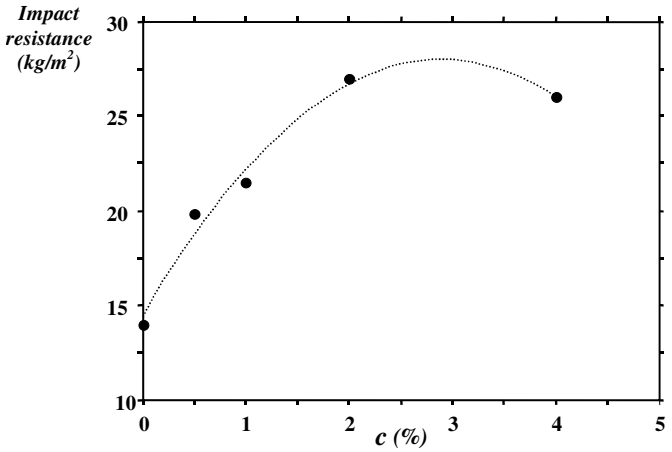

Figure 10. Impact resistance versus the coating level of hydrogenated tallow amine c (%).

sphere suspensions and the break-up process of the aggregates [15, 31–34]. Recent computer simulations [35, 43] and experimental studies [36, 44–46] of the break-up of aggregates in shear or elongational flow are often limited to the diluted regime and neglect the hydrodynamic interactions between aggregates.

We consider in this section the microrheological model proposed by Snabre and Mills [15] based on a reference viscosity law describing the Newtonian behaviour of hard spheres in purely hydrodynamic interactions [27, 28]:

$$\frac{\mu(\phi)}{\mu_0} = \frac{1-\phi}{(1-\phi/\phi^*)^2} \tag{34}$$

where μ is the viscosity of the non-aggregated suspension, μ_0 is the viscosity of the suspending medium and ϕ^* is the maximum packing fraction of the structural units.

The polymeric fluid further exhibits Newtonian behaviour at low shear rates and shear-thinning behaviour at high shear rates of deformation [47]. We may thus consider the viscoelastic properties of the polymeric matrix by introducing the Bird–Carreau expression in equation (34):

$$\mu_0(\dot\gamma) = \mu_{0m}[1 + (C\dot\gamma)^2]^{(n-1)/2} \tag{35}$$

where μ_{0m} is the zero-shear-rate viscosity of the matrix polymer and C is a constant related to the onset of shear thinning.

In the case of particle aggregation, the suspension shows a yield stress above the gelation threshold ϕ_g because of the formation of an infinite spanning network which displays a solid-like viscoelasticity behaviour [22]. At rest, fractal structures then fill space and reach a maximum size $\hat R(\phi)$ which decreases with particle volume fraction [15,27,28]. The suspension may then be considered as a collection of fractal subclusters of mean density ϕ and size $\hat R(\phi) \approx a(\phi/\phi^*)^{1/(D-3)}$ packed with a volume fraction ϕ^*.

Above the yield shear stress τ_0, the space-filling subclusters of size $\hat R(\phi)$ are broken into smaller clusters and the suspension may flow. The condition $R(\tau) = \hat R(\phi)$ then gives an expression for the yield shear stress τ_0:

$$\tau_0 \approx \tau^*\left[\left(\frac{\phi}{\phi^*}\right)^{1/(D-3)} - 1\right]^{-1/m} \qquad \text{for } \phi > \phi_g. \tag{36}$$

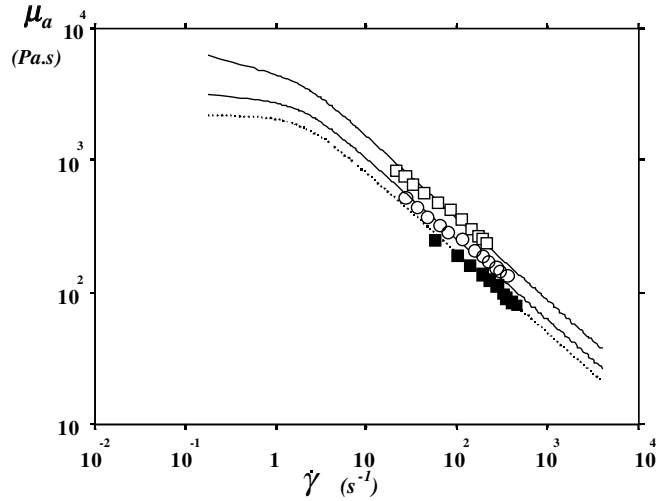

Figure 11. Shear viscosity $\mu_a(\dot{\gamma})$ versus the shear rate $\dot{\gamma}$ for untreated silica fumes in polypropylene. Filler volume fraction $\phi = 0.08$ (○) and $\phi = 0.17$ (□). The dashed curve represents the viscosity of the unfilled polymer $\phi = 0$ (■). The solid curves are calculated from the microrheological model.

The shear-thinning behaviour of flocculated suspension arises from the ability of clusters to screen the shear field and trap the interior fluid. For a fractal dimension $D > 2$, clusters may be considered as impermeable with strong hydrodynamic screening inside the aggregates. Above the yield stress, the finite-size clusters then behave like compact spheres of radius $R(\tau)$ and the viscous dissipation in the fluid between the aggregates determines the effective viscosity of the suspension. Therefore, we may introduce the effective volume fraction ϕ_a of clusters and use the reference viscosity law (equation (34)) to estimate the shear viscosity $(\mu_a(\phi, \tau)/\mu_0) = (1 - \phi_a)/(1 - \phi_a/\phi^*)^2$ of the flocculated suspension with $\phi_a(\tau) = \phi(R(\tau)/a)^{3-D}$.

The effective-medium approximation was established from rheo-ultrasonic experiments [12, 23]. As a consequence, we may consider that interacting clusters behave like isolated aggregates in a fluid of viscosity equal to the shear viscosity of the suspension and thus experience an effective shear stress $\tau = \mu_a(\phi, \tau)\dot{\gamma}$. Equations (35) and (36) together, and the estimate of the shear viscosity of the aggregated suspension with the condition $\tau = \mu_a(\dot{\gamma})\dot{\gamma}$, then give a non-linear expression for the effective viscosity. For a fractal dimension $D = 2$, the rheological equation then takes the form [15]

$$\sqrt{\tau}\left[1 - \left(\frac{\tau_0}{\tau}\right)^m\right] = \sqrt{\mu\gamma}\left[1 - \frac{\phi}{1-\phi}\left(\frac{\tau^*}{\tau}\right)^m\right]^{1/2} \tag{37}$$

with

$$\mu = \mu_0(\dot{\gamma})\frac{1-\phi}{(1-\phi/\phi^*)^2} \tag{38}$$

where τ^* is the critical disaggregation shear stress and μ the viscosity of the dispersed suspension in the high-shear regime.

Taking $C = 1.5, n = 0.39$ and $\mu_{0m} = 2.2\,\mathrm{kPa\,s^{-1}}$, the Bird–Carreau model (equation (36)) describes well the shear viscosity of the unfilled PP homopolymer (figure 11). We have further determined the shear viscosity $\mu_a(\dot{\gamma})$ of untreated silica fumes in suspension in PP

homopolymer. On increasing the shear rate, clusters are progressively broken and the viscosity decreases because of the lower fluid volume fraction trapped in the aggregates. For filler volume fraction close to 0.08, the shear viscosity still exhibits a Newtonian behaviour at low shear rates. As the filler volume fraction increases, a yield stress becomes apparent.

Viscoelastic properties of the polymeric matrix further dominate the rheological behaviour in the higher-shear regime (figure 11). Assuming rigid clusters ($m = 1/3$) of fractal dimension $D = 2$ and from the critical shear stress τ^* determined by ultrasonic experiments, we further describe the shear-thinning behaviour of filled PP homopolymer with untreated silica fume particles. The viscosimetric method thus confirms that silica fume aggregates can be considered as rigid clusters. Both the scattering and viscosimetry methods can give an estimate of the disaggregation shear stress τ^* representative of the mechanical force required to disrupt the bonds between particles. However, the critical disaggregation shear stresses τ^* determined from rheo-acoustic and viscosimetric experiments differ by a factor of 10. The viscosimetric method probably underestimates the critical disaggregation shear stress τ^*, since particle aggregation dominates the rheological behaviour in the low-shear regime and the shear viscosity is not very sensitive to the presence of small aggregates.

6. Conclusions

In the present study, a rheo-acoustic approach for investigating the shear break-up processes of fractal polydisperse fillers has been proposed and applied to silica fume aggregates under well defined hydrodynamic conditions. Within the framework of fractal aggregation, the ultrasound scattering power from a dense distribution of irreversible Rayleigh polydisperse clusters is nearly isotropic. Far-field coherence effects and polydispersity of the scatterers together determine the cluster volume dependence of the dimensionless ultrasonic scattering coefficient without dependence on filler volume fraction, fractal dimension of the aggregates or particle size distribution because the ultrasonic wave cannot resolve the internal structure of aggregates smaller than the wavelength. The ultrasound scattering technique has the main advantage of being only sensitive to cluster volume, whatever the internal structure of the clusters. The rheo-acoustic model for cluster break-up describes the ultrasonic experiments well. The flow-dependent changes of the ultrasound scattered power from silica fume clusters support the use of the effective-medium approximation in the microrheological models. The shear stress dependence of the dimensionless ultrasonic scattering coefficient further indicates that silica fume aggregates can be considered as rigid clusters ($m = 1/3$) with a fractal dimension $D = 2$, since small elastic deformations are transmitted over the whole structure and then preserve the structure of rigidly connected particles in relation to irreversible aggregation. The ultrasound scattering technique is better suited for determining the critical disaggregation shear stress of silica fume suspensions in relation to the surface treatment of the fillers. Good correlations are further obtained when comparing ultrasonic experiments, either static or during flow, with impact tests. This study clearly demonstrates that the rheo-acoustic method provides a powerful means for examining the mean-field approximation used in the microrheological models and analysing the break-up processes of fractal clusters in a shear field. From the microrheological model and measurements of the disaggregation shear stress, the shear-thinning behaviour of silica fume clusters is fairly well described.

References

[1] Birley A W, Haworth B and Batchelor J 1992 *Physics of Plastics* (New York: Hanser)
[2] Osswald T A and Menges G 1995 *Materials Science of Polymers for Engineers* (New York: Hanser)

[3] Challis R E, Tebbut J S and Holmes A K 1998 *J. Phys. D: Appl. Phys.* **31** 3481–97
[4] Allegra J R and Hawley S A 1971 *J. Acoust. Soc. Am.* **51** 1545–64
[5] Rayleigh J W S 1945 *Theory of Sound* (New York: Dover) 414–31
[6] Mo L Y L and Cobbold R S C 1993 *Ultrasonic Scattering in Biological Tissues* ed K K Shung and G A Thieme (Boca Raton, FL: Chemical Rubber Company) pp 125–71
[7] Lucas R J and Twersky V 1987 *J. Acoust. Soc. Am.* **82** 794–9
[8] Shung K K, Cloutier G and Lim C C 1992 *IEEE Trans. Biomed. Eng.* **39** 462–9
[9] Hanss M and Boynard M 1979 *Ultrasonic Tissue Characterization* part 2, vol 525, ed M Linzer (Washington, DC: National Bureau of Standards) pp 165–9
[10] Twersky V 1988 *J. Acoust. Soc. Am.* **84** 409–15
[11] Berger N E, Lucas R J and Twersky V 1991 *J. Acoust. Soc. Am.* **89** 1394–401
[12] Haïder L, Snabre P and Boynard M 2000 *J. Acoust. Soc. Am.* **107** 1715–26
[13] Mandelbrot B B 1982 *The Fractal Geometry of Nature* (New York: Freeman)
[14] Mo L Y L and Cobbold R S C 1992 *IEEE Trans. Biomed. Eng.* **39** 450–61
[15] Snabre P and Mills P 1996 *J. Physique* **6** 1811–34
[16] Snabre P and Mills P 1996 *J. Physique* **6** 1835–55
[17] Morse P M and Ingard K U 1968 *Theoretical Acoustics* (New York: McGraw-Hill)
[18] Twersky V 1962a *J. Math. Phys.* **3** 700–15
Twersky V 1962b *J. Math. Phys.* **3** 724–34
[19] Twersky V 1978 *J. Acoust. Soc. Am.* **36** 1710–19
[20] Twersky V 1987 *J. Acoust. Soc. Am.* **81** 1609–14
[21] Kolb M and Jullien R 1984 *J. Physique Lett.* **45** L977–81
[22] Weitz D A and Huang J S 1984 *Aggregation Gelation* ed F Family and D P Landeau (Amsterdam: North-Holland) p 19
[23] Snabre P, Haïder L and Boynard M 2000 *Eur. Phys. J.* E **1** 41–53
[24] Snabre P, Haïder L and Mills P 1999 *Cah. Rhéol.* **16** 20–9
[25] Lin M Y, Klein R, Lindsay H M, Weitz D A, Ball R C and Meakin P 1990 *J. Colloid Interface Sci.* **137** 263–80
[26] Fisher M E and Burford R 1967 *Phys. Rev.* **156** 583–622
[27] Mills P 1985 *J. Physique Lett.* **46** L301–9
[28] Mills P and Snabre P 1988 *Rheol. Acta* **26** 105–8
[29] Sonntag R C and Russel W B 1987 *J. Colloid Interface Sci.* **115** 378–89
[30] Patel P D and Russel W B 1988 *Colloids Surf.* **31** 355–83
[31] Potanin A A and Uriev N B 1991 *J. Colloid Interface Sci.* **142** 385–95
[32] Wessel R and Ball R C 1992 *Phys. Rev.* A **46** R3008–11
[33] Potanin A A, De Rooij R, Van Den Ende D and Mellema J 1995 *J. Chem. Phys.* **102** 5845–53
[34] Wolthers W, Duits M H G, Van Den Ende D and Mellema J 1996 *J. Rheol.* **40** 799–811
[35] Potanin A A 1993 *J. Colloid Interface Sci.* **157** 399–410
[36] Torres F R, Russel W B and Schowalter W R 1991 *J. Colloid Interface Sci.* **145** 51–73
[37] Bossis G, Meunier A and Brady J F 1991 *J. Chem. Phys.* **94** 5064–70
[38] Piché L, Massines F, Hamel A and Néron C 1988 *US Patent Specification* 4,754,645
[39] Piché L, Hamel A, Gendron R, Dumoulin M M and Tatibouët J 1995 *US Patent Specification* 5,433,112
[40] Bird R B, Armstrong R and Hassager O 1987 Dynamics of polymeric liquids *Fluid Mechanics* vol 1 (New York: Wiley)
[41] Derjaguin B V, Muller V M and Toporov Y P 1975 *J. Colloid Interface Sci.* **53** 314–26
[42] De Gennes P-G 1981 *Scaling Concepts in Polymer Physics* (Ithaca, NY: Cornell University Press)
[43] Jullien R and Botet R 1987 *Aggregation and Fractal Aggregates* (Singapore: World Scientific)
[44] Higashitani K and Iimua K 1997 *J. Colloid Interface Sci.* **204** 320–7
[45] Oles V 1992 *J. Colloid Interface Sci.* **154** 351–8
[46] Yeung A K C and Pelton R 1996 *J. Colloid Interface Sci.* **184** 579–85
[47] Serra T, Colomer J and Casamitjana X 1997 *J. Colloid Interface Sci.* **187** 466–73